B vs H Narrative

An electronic test fixture was prepared for analyzing the dynamic magnetic field versus current excitation, or **B** versus **H**, of our chosen yoke and armature laminations. The fixture included a data acquisition system for generating excitation waveforms and sampling data; power amplification driving the main coil; a secondary coil for flux sensing, and current sensing. Flux was determined by analog integration of the sense coil voltage. Test results were scaled to SI units: flux density **B** in Teslas and excitation **H** in Amps/Meter. **B** and **H** are readily translated into flux, **Φ**, and winding current, **I**. Fig. 1 shows the basic B versus H graph:

Fig. 1

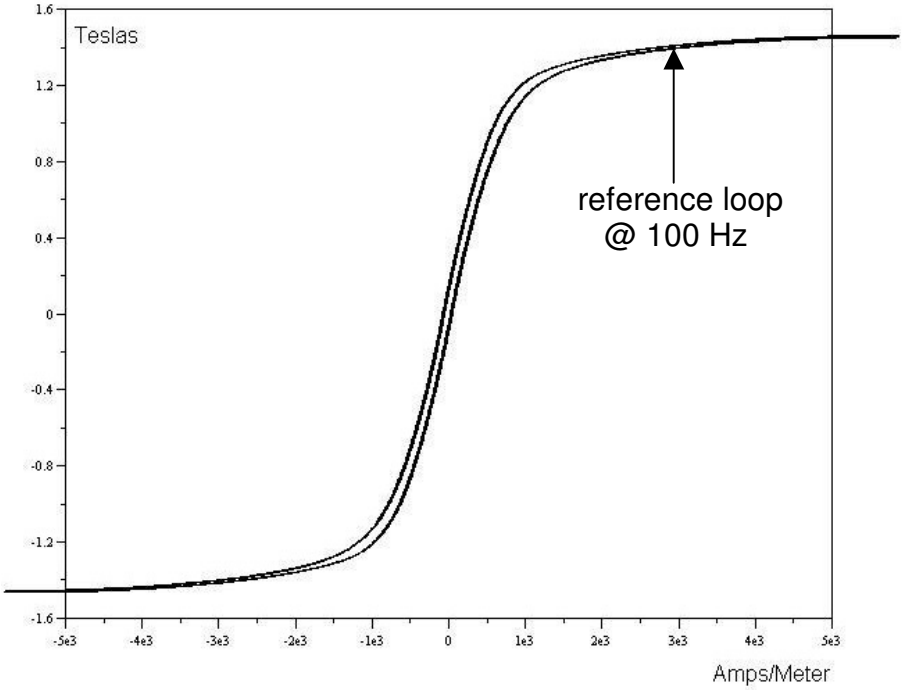

Overall hysteresis is attributed partly to magnetic hysteresis and partly to eddy currents, the eddy current effect being somewhat larger at 100 Hz and dominant at higher frequencies. The Fig. 1 trace is shown for the armature clamped tightly to the yoke for the smallest practical magnetic gap. That minimum effective gap is non-zero, since lamination edges do not fit perfectly flat. The effective magnetic air gap here is about 0.00085 inches or .0216 mm. Fig. 2, on the next page, models the change in the **B** vs **H** loop after adding a .005 inch (0.127 mm) separation between the yoke and armature. The hysteresis loop with the steeper middle portion is the same the reference loop of Fig. 1. The flatter hysteresis loop is computed, starting from the reference loop and re-scaling the horizontal, H-field coordinates, to model the additional H-field needed to carry the magnetic flux across the air gap as well as through the lamination metal. Note that while the permeability of the ferromagnetic metal is nonlinear, the permeability of the air gap is linear. The air gap linearity results in a more nearly linear **B** vs **H** graph where the air gap is present. Note also that according to the theory used to generate the second graph, the absolute horizontal width of the hysteresis loop is unchanged from the zero-gap graph.

Fig. 2

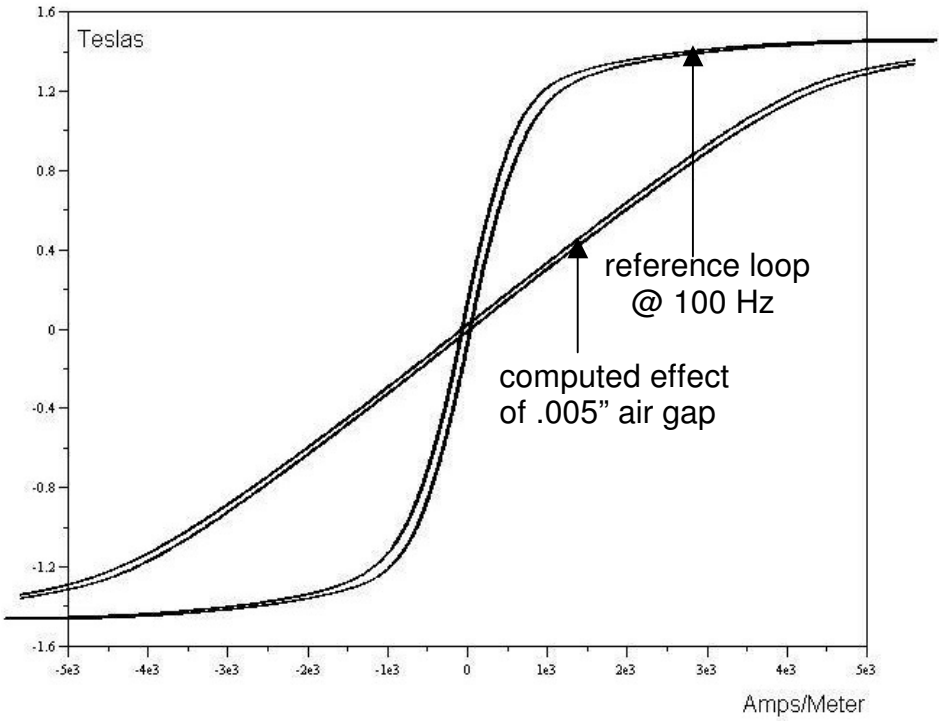

In Fig. 3, the hysteresis curve computed for a .005 inch (0.127 mm) gap is plotted on an expanded horizontal scale and compared with an empirically measured hysteresis loop, plotted on the same axes. The empirically measured curve exhibits magnetic saturation at a lower maximum B-field that was expected from the formula used for Fig. 3, which retained the saturation characteristics of the original reference loop.

Fig. 3

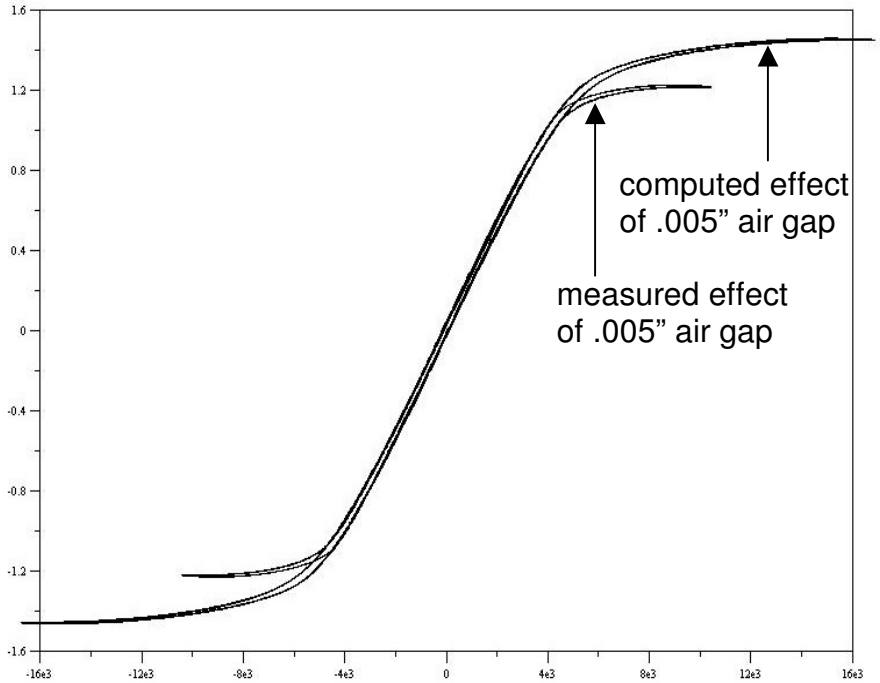

Comparing the theoretical and measured curves of Fig. 3, the correlation is excellent except at high flux levels, where saturation sets in at a lower level in the measured curve. Similar results were obtained by Bergstrom in an independent study using two-dimensional magnetic Finite Element Analysis (FEA) to demonstrate an earlier onset of saturation with an air gap. While the FEA approach differs systematically from real data because it fails to model "end effects" that would require a full 3-D analysis, the FEA model aids in understanding the trends described here. The trend toward lower apparent saturation is explained by a less uniform spatial distribution of the magnetic field when an air gap opens. In these analyses, the field strength value "**B**" is actually computed from the total magnetic flux linking the coil windings, averaged over the winding volume. When an air gap opens up at the gap end of the winding, an increasing amount of flux "short circuits" across air gaps in the yoke, failing to bridge across to the armature and failing to pass through some of the windings. Thus, the average B-field linking the windings is lower that the local B-field occurring in the backs of the E-core yoke laminations, on the far side from the air gap. The field strength in the backs of the laminations becomes the "bottleneck" limiting magnetic flux.

The important practical result of these saturation effects is to limit the force of magnetic attraction at magnetic saturation. A family of B versus H curves like the measured curve in Fig. 3 provides a complete picture of how magnetic energy varies as a function of armature position. With this information alone, it is possible to compute magnetic force on the armature, including in nonlinear situations. These force results are then grounded in empirical data obtained without the necessity of force measurement.

Fig. 4 compares hysteresis loops at 100 and 200 Hz, the higher-frequency loop being offset to the right for a side-by-side comparison. The horizontal scale is not labeled, since each point represents two different values, one for each graph. The horizontal scales in fact match those of Figs. 1 and 2. It is seen that a doubling of frequency causes slightly less than a doubling in hysteresis width, indicating that hysteresis is caused predominantly by eddy currents at these frequencies and in these .014 inch thick laminations.

Fig. 4

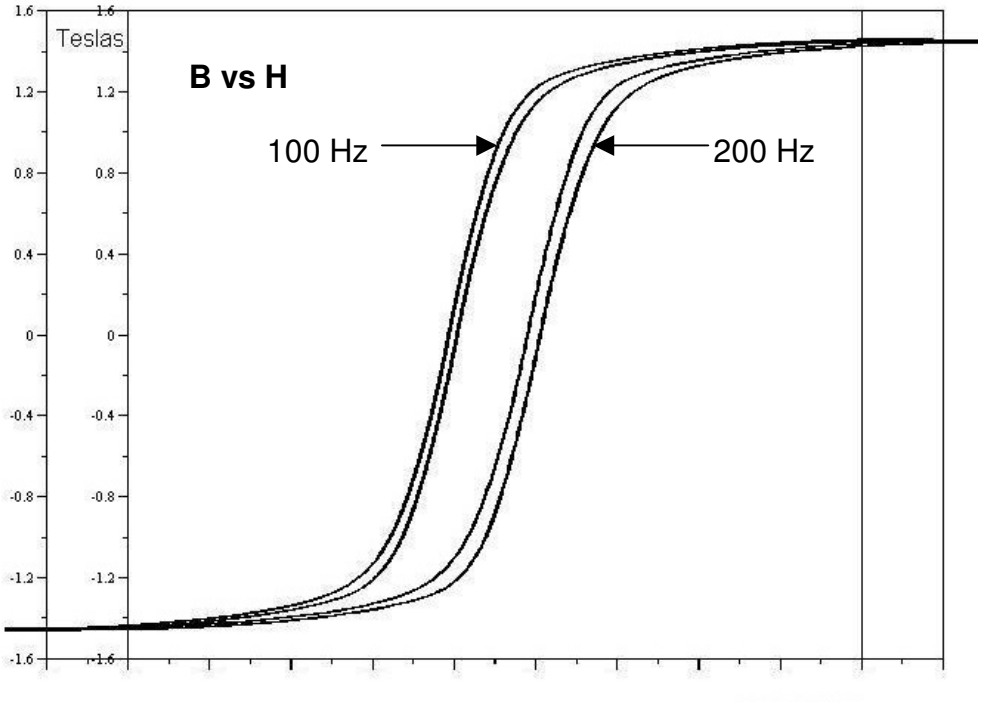

When the magnetic field is changed at a variable rate, quickly, then slowly, then quickly again, the effect of eddy currents varies approximately in proportion to the instantaneous rate-of-change of the B-field. The accuracy of this approximation is tested as follows. A sinusoidal 50 Hz inductive drive waveform was altered by the addition of an 800 Hz waveform, varying in amplitude so that the rate of change of magnetic flux, or dB/dt, would be altered strongly but not so much as to cause a change in direction. Phase distortions in the experiment caused dB/dt to change sign near saturation but to remain monotonic with a large fractional variation while B ramped up from zero to the vicinity of saturation. A graph of B-versus-time is shown in Fig. 5:

Fig. 5

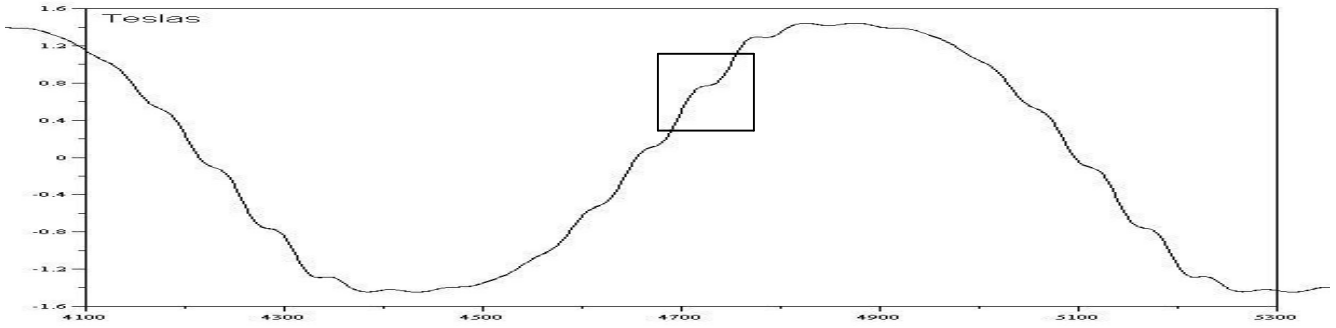

Just above the center of the graph, in the boxed area, the rate of increase of B is seen to slow almost to a stop in the vicinity of 0.8 Teslas, while the slope is relatively steep on either side. Fig. 6a, below on the left, shows the uncorrected effect of this alteration in slope on the graph of B versus H. This graph shows side-by-side traces without and with the 800 Hz ripple signal. The “kinked” graph is offset to the right – otherwise the two graphs would overlap. By simulating a compensatory eddy current path with negative resistance, the kink in the curve is reduced but not completely removed, as shown in the graph in Fig. 6b, on the right.

Fig. 6a

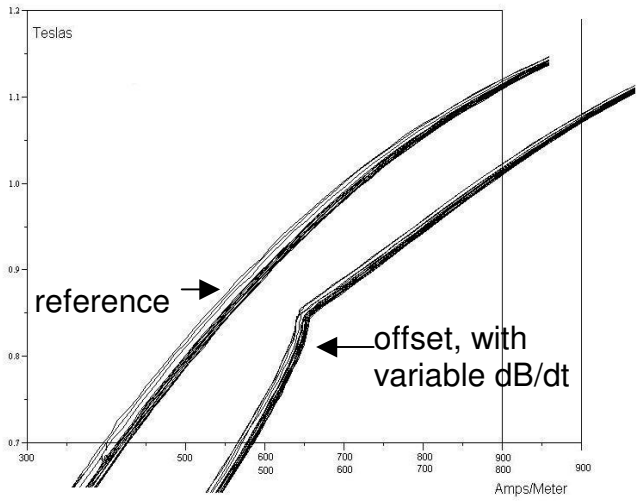

Fig. 6b

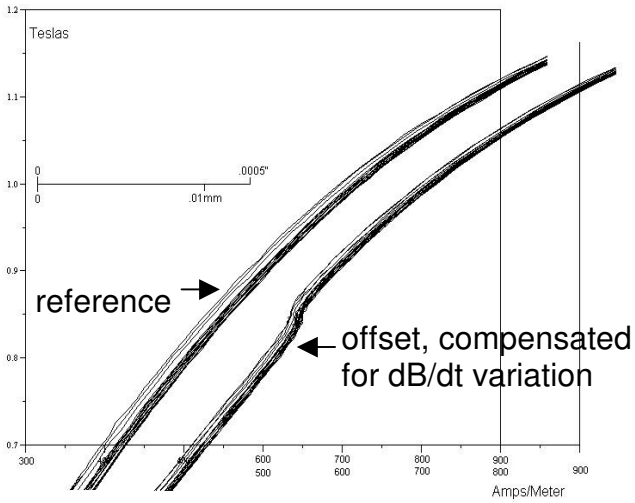

Similar sets of graphs were obtained for a greater 800 Hz modulation amplitude, causing the direction of change in the B-field to reverse on the way from the most negative to the most positive extremes. The following graphs illustrate B as a function of time (Fig. 7), uncompensated B versus H (Fig. 8a) , and compensated B versus H (Fig. 8b), using the same eddy current correction as for the lesser 800 Hz modulation shown above. Note that both the horizontal and vertical scales of Figs. 8a and 8b cover a much broader range than in Figs. 6a and 6b.

Fig. 7

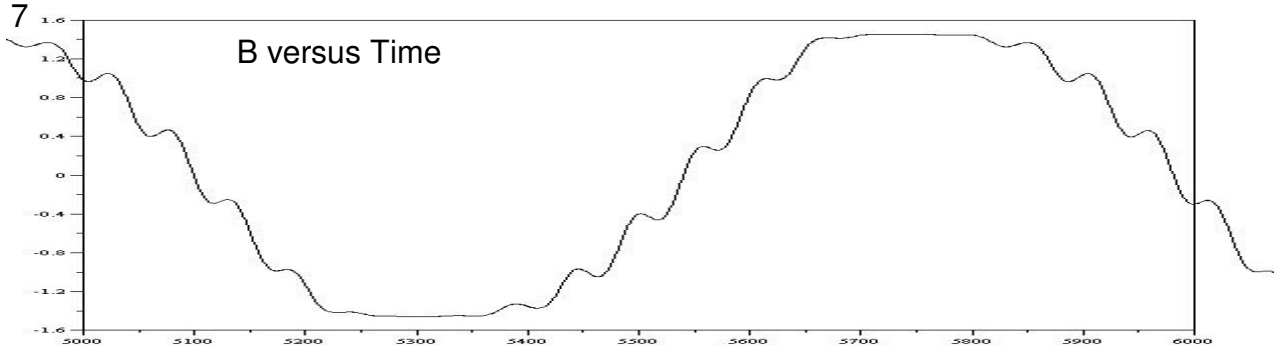

Fig. 8a

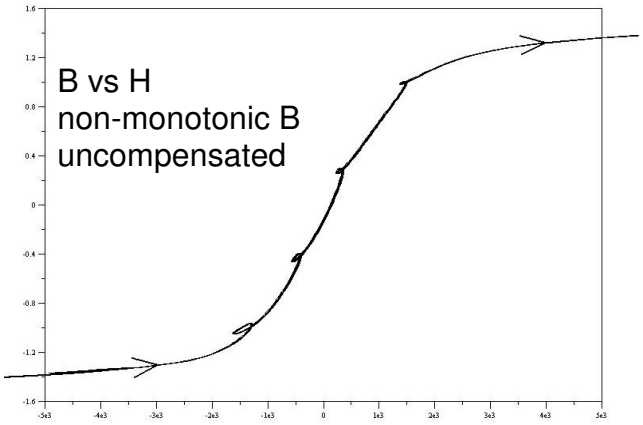

Fig. 8b

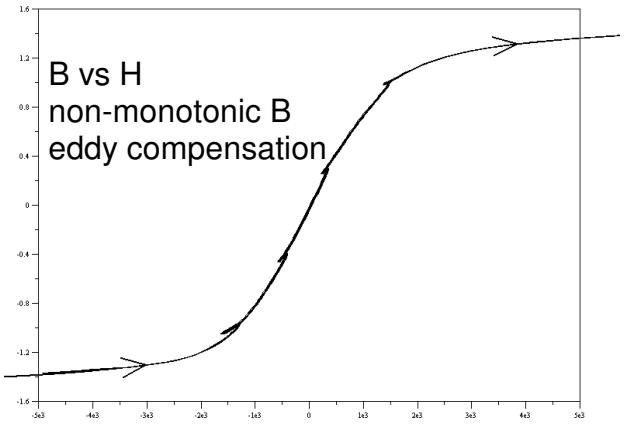

While eddy current compensation is fairly effective at removing the kinks from the B versus H graph when the change in B is monotonic, the graphs of Figs. 8a and 8b illustrate that eddy current compensation is not nearly as effective when B is non-monotonic. Reversals in the direction of change of B introduce hysteresis errors.

For the Magnesense servo control approach, distance is inferred from the ratio H/B, or equivalently, from the ratio current/flux. The sensitivity of this distance scale is indicated in Fig. 6b (above) at a reference B-field of 1.0 Tesla. The scale indicates a distance of 0.1 millimeters on the bottom and .0005 inches on the top. The wrinkle in the B versus H curve caused by a reduction in rate almost to zero is seen to amount to a position uncertainty of very roughly .001 millimeters or .00004 inches. This error sensitivity, illustrated for a nearly closed magnetic gap, remains about the same for larger gaps in the range of interest. When the B-field slope ripple is roughly doubled, causing a non-monotonic increase in B as

illustrated above in Fig. 7, then the maximum position error increases by roughly a factor of ten, to about .01 millimeters or .0004 inches.

The above data, applied to the design of a sensorless valve actuation system, pertain to two engineering design concerns:

- reduced magnetic pull at a distance caused by lower magnetic saturation limit; and,
- less precise servo control for sensorless soft landing.

Magnesense has developed empirical formulas from the results shown above and incorporated those formulas into dynamic simulation models. A working solenoid system, including sensorless control, has been developed from these models. The system works. It uses sensorless determination of position and velocity to stabilize dynamic trajectories and bring about soft landings. The theory predicts that, for the current system, we should not be running into significant magnetic saturation problems. Since our sensorless system for computing armature position is sensitive to saturation, we would immediately recognize saturation, even at incipient levels. As predicted based on the above data, saturation is not a problem with our present operating envelope. Similarly, the data above predict measurable effects from eddy currents and magnetic hysteresis. Both kinds of effect are observable in our system and make enough difference to merit first-order correction formulas. Thus, our control algorithm includes a resistive shorted turn model to correct for eddy currents, and it includes an ampere-turn offset term to compensate for hysteresis when the flux linkage is increasing monotonically on a trajectory to armature landing and latching. When our dynamic trajectories cause departures from a non-monotonic increase in magnetic flux, our computations of position are thrown off a little bit while our finite-difference computations of velocity are thrown off sufficiently to cause problems in our feedback control process. In other words, these models are more than academic. They work, and they help us to understand what is going on in our practical control system development. Using sensorless inference of position and maintaining a monotonic increase in flux linkage for a closing solenoid, we are able to achieve consistent armature landings with impact velocities below .05 meters/second. As we redesign our system to meet greater performance demands in a smaller physical package, we will increasingly encounter the kinds of non-ideal magnetic characteristics discussed in this paper. Some level of understanding of these effects is a valuable asset for practical design.